

## Characterizing solute transport in undisturbed soil cores using electrical and X-ray tomographic methods

P. A. Olsen,<sup>1\*</sup> A. Binley,<sup>2</sup> S. Henry-Poulter<sup>2</sup> and W. Tych<sup>2</sup>

<sup>1</sup>*Department of Soil and Water Sciences, Agricultural University of Norway, Ås, Norway*

<sup>2</sup>*Institute of Environmental and Natural Sciences, Lancaster University, Lancaster, UK.*

---

### Abstract:

Solute transport in undisturbed soil is a complex process and detailed information on the transport characteristics is needed to provide fundamental understanding of the processes involved. X-ray computer tomography (CT) and electrical resistivity tomography (ERT) have been used to gain information on the transport characteristics. Both methods are non-intrusive and do not disturb the soil, in contrast to other methods. CT provides high resolution information on bulk density and macropores, while ERT provides a three-dimensional image of the internal resistivity structure. By adding a suitable solute under steady-state flow, the internal resistivity changes can be interpreted as a change in resident concentrations. In our experiment two cores from different field sites were investigated. The ERT measurements revealed two transport modes (one fast and one slow) in one of the cores and only one mode in the other. This was consistent with the results of transfer function modelling on the independently measured breakthrough curves (BTCs). The fast transport mode is perhaps a result of many connected macropores, detected by CT, but this could not be verified with the ERT measurements because of the coarser resolution. However, with ERT in both cases we were able to explain the observed BTC qualitatively. Copyright © 1999 John Wiley & Sons, Ltd.

**KEY WORDS** X-ray computer tomography; electrical resistivity tomography; undisturbed soil cores; solute transport; breakthrough curves; transfer functions

### INTRODUCTION

There has been a great deal of recent interest in the solute transport characteristics of naturally occurring geological materials, owing to the increasing concern about water quality. The European Environment Agency and United Nations Environmental Program (1997), for example, reports that model calculations estimate that water lying beneath more than 85% of agricultural land has a higher level of nitrate than the European Union guidelines for nitrate concentration in drinking water. Particular difficulties that may occur both in measuring and modelling transport processes are caused by preferential flow and scale-dependent dispersion. There is a pressing need to know more about these processes and how soil structure and heterogeneous material affect solute flow. In order to address these questions, detailed information on solute movement is essential. Traditionally, change in solute concentration is measured by inserting suction cups,

---

\* Correspondence to: Dr Per Atle Olsen, Department of Soil and Water Sciences, Agricultural University of Norway, PO Box 5028, 1432 Ås, Norway.

Email address: P. A. Olsen (per-atle.olsen@ijvf.nlh.no).

Contract grant sponsors: European Groundwater Research Network, EC; Norwegian Research Council.

Contract grant numbers: ERB CHRX CT92 0074; 116146/100.

time domain reflectometry probes or conductivity probes into the material. These techniques provide relatively local, or even point, estimates of solute behaviour. In addition, these methods are truly invasive thus possibly disturbing the flow itself. New methods that are non-destructive or non-intrusive are therefore needed.

X-ray computerized tomography (CT) has been used to study the internal structure of soil and sediments for some years (see, for example, Anderson and Hopman, 1994). It has also been successfully used in the investigation of solute transport properties. The equipment necessary for X-ray CT, since it was not developed for environmental applications, has many limitations when used for this purpose. The sample size is restricted by the penetration depth of the X-rays, the experimental set-up is determined by the size of the CT equipment and the equipment is very expensive and seldom available for time-consuming experiments. Magnetic resonance imaging (MRI) techniques have also been used to characterize water in porous media. MRI provides high resolution images, but problems may occur in obtaining high quality images of very heterogeneous materials owing to variations in magnetic susceptibility within the sample (Amin *et al.*, 1997). MRI also requires expensive equipment and, like CT, is limited in its scale of application. In an attempt to provide a more flexible and relatively inexpensive tool for preliminary biomedical investigations, electrical impedance tomography was developed during the 1980s (see, for example, Barber and Brown, 1984). Methods based solely on mapping resistive components of impedance have been labelled electrical resistivity tomography (ERT) and have been shown to have value in environmental contexts (see, for example, Binley *et al.*, 1996a). The soil samples can be larger than for CT and MRI experiments, allowing the investigation of more structural units. ERT may also be used at the field scale by imaging solute behaviour between boreholes (Daily *et al.*, 1992; Slater *et al.*, 1996).

Recent developments in resistivity imaging has led to fully three-dimensional inversion procedures (see, for example, Binley *et al.*, 1996b). Here we utilize both three-dimensional ERT and X-ray tomography to assess the hydraulic and transport characteristics of soil cores taken from two field sites. The images obtained are compared with respect to features relating to hydraulic properties. A classical tracer experiment is then conducted and we wish to explain the observed breakthrough curves with the aid of our CT and ERT measurements.

## MATERIALS AND METHODS

### *X-ray computer tomography*

CT makes use of the attenuation of X-rays passing through a material. This attenuation increases with increasing density and increasing atomic number of the material in the object. Measurements from different angles are reconstructed to obtain an image of the internal density or chemical composition (Anderson and Hopman, 1994).

A Siemens SOMATOM 2 system was employed to investigate the internal features of the two soil columns. Each core was scanned in 4-mm slices perpendicular to the longitudinal axis and in 1-cm intervals from top to bottom. Each image thus reflects the average of the attenuation in the 4-mm slice and is presented in a  $256 \times 256$  matrix as computerized tomography densities (CTD). The CTDs are the attenuation coefficients ( $\mu$ ) calibrated against water. CTDs are also frequently called Hounsfield units.

$$CTD = K \frac{\mu - \mu_{\text{water}}}{\mu_{\text{water}}}$$

$K$  is a constant usually equal to 1000. Consequently, water has the value of 0 and air, which has a negligible attenuation coefficient, has the value  $-1000$ . The attenuation, and hence CTD, is linearly related to soil bulk density. The resolution, i.e. the size of detectable features, depends on the contrasts in CTD and approaches 1 mm for high contrasts.

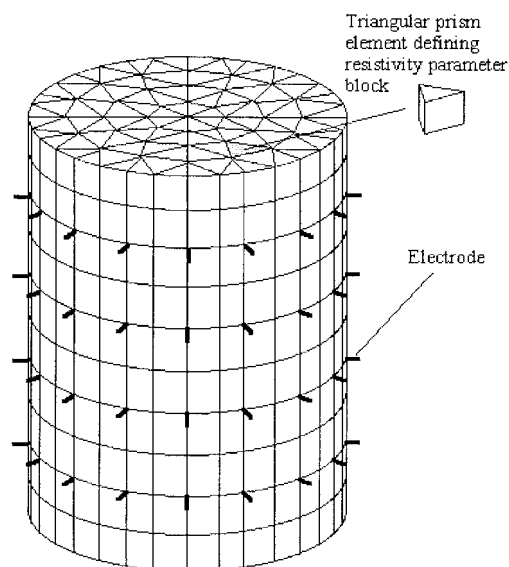


Figure 1. Electrode positions and finite element mesh of the soil cores

### Electrical resistivity tomography

By placing electrodes around the body under investigation, measurement of voltages between pairs of electrodes as a response to injected current between another pair of electrodes provides a transfer resistance. The purpose of ERT is to determine the internal resistivity structure from these boundary transfer resistance measurements. To achieve this, non-linear inverse methods may be used to reconstruct the three-dimensional image of resistivities (Binley *et al.*, 1996b).

Figure 1 shows, schematically, the arrangement adopted here. Electrodes are placed in four equidistant planes with 16 electrodes evenly spaced on the circumference. The region (the soil core) is discretized into a number of triangular prism finite elements. These finite elements permit the definition of the spatial distribution of resistivity within the core and allow computation of the theoretical measurements owing to such a structure. By means of an iterative inversion procedure, the resistivity structure is determined that best fits the measured response.

Satisfactory image reconstruction relies on estimates of the error in the transfer resistance measurements. Pre-processing of the collected transfer resistances gives an estimate of the data uncertainty which is used to weight the measurements during the inversion procedure. A frame is the complete set of measurements for all 64 electrodes. For the experiments reported, a frame consists of 1600 transfer resistances, taking about 4.5 hours to collect. By dividing the core into 10 planes, each subdivided into 104 triangular prisms (Figure 1), the result is a three-dimensional image of 1040 resistivity values.

### Estimating transport parameters

By measuring the internal bulk electrical resistivities at different times we are able to investigate the transport of an electrically conductive solute as it migrates through the core. In order to do this a model relating the solute conductivity to the bulk electrical resistivity is required.

A very simple analytical model is to regard the solute as a number of parallel conductors with conductivity  $\sigma_s$  in a solid matrix with conductivity  $\sigma_m$  and volume fraction  $f$ . The effective bulk electrical conductivity is thus  $\sigma_b = f\sigma_m + (1 - f)\sigma_s$ , which is related to the bulk resistivity by  $\rho_b = \sigma_b^{-1}$ . Empirical relationships such as Archie's law,  $\sigma_b = S^k FF\sigma_s$  are more common. Here  $S$  is the degree of saturation,  $k$  an empirical factor and  $FF$  a formation factor. Both models give a linear relationship between the bulk electrical conductivity

and the fluid conductivity. Hence a reasonable assumption is that the change in the bulk conductivity is proportional to the change in the fluid conductivity. In the range of solute concentration used here (0.01–0.05 M KCl) there is also a linear relationship between fluid conductivity and solute concentration. The change in bulk resistivity is thus interpreted as a change in solute concentration. In this way the breakthrough curves (BTCs) of the different voxels can be investigated.

ERT measures a volume average resistivity which corresponds to a resident concentration (Parker and van Genuchten, 1984) and provides a spatial distribution of conductivities at chosen times. At the outlet, measurement of the electrical conductivity of the effluent corresponds to a flux concentration and thus we have a temporal distribution at one specific depth (the outlet). When working with volume-averaged conductivities (resident concentrations) we can also average over a larger volume. In order to assess the vertical distribution of the resident concentrations, the average over each plane may be computed and thus produce one-dimensional resident concentration profiles at different times.

In order to estimate transport parameters that are independent of a process model we have chosen to adopt the transfer function model of Beven and Young (1989). It is possible to show that a solution of any linear differential equation, as for instance the convection dispersion equation (CDE), is

$$c(t) = \int_0^t u(\tau)i(t - \tau) d\tau$$

where  $c$  is the response of an input  $i$  at earlier times ( $t - \tau$ ) and  $u(\tau)$  is the impulse response function, as in the transfer function approach of Jury and Roth (1990). The discrete version of this integral is generally an infinite series,  $c_k = \sum_j v_j i_{k-j}$ . This merely states that the response ( $c_k$ ) at time-step  $k$  is a linear combination of earlier inputs,  $j$ . A time delay can be introduced by letting the first  $d$  coefficients be zero. By introducing the backward shift operator ( $z^{-1}$ ) defined as  $z^{-1}c_k = c_{k-1}$  (Young, 1984), the discrete version may be written as an infinite series of  $z^{-1}$ . A parsimonious representation (more effective with respect to the number of coefficients  $v$ ) is to write the infinite sum as a ratio of two polynomials in  $z^{-1}$

$$c_k = \frac{b_0 + b_1 z^{-1} + b_2 z^{-2} + \dots + b_n z^{-n}}{1 + a_1 z^{-1} + a_2 z^{-2} + \dots + a_m z^{-m}} i_{k-d}$$

This general model is referred to a model of order  $[m, n, d]$ . We do not yet have to specify a process model because so far this is a completely data-based model and the only assumption is that of a linear system. The model order has to be determined from the experimental data.

If we want to connect the parameter vectors  $\mathbf{a}$  and  $\mathbf{b}$  to physical quantities we must make some assumptions and specify a differential equation. The parameter vector  $\mathbf{a} = [1, -0.9, 0.8]$ , for instance, denotes the polynomial  $1 - 0.9z^{-1} + 0.8z^{-2}$ . A fundamental assumption is that the mass balance is fulfilled. The balance of mass can be written in terms of the steady-state flow rate ( $Q$ ), the effective volume of transport ( $V_e$ ) and the concentration for the output [ $c(t)$ ] and the input [ $i(t - \tau)$ ], where  $\tau$  is the time delay

$$\frac{dc}{dt} = \frac{Q}{V_e} [i(t - \tau) - c(t)]$$

The discrete version of this equation is  $c_k = -ac_{k-1} + bi_{k-d}$ , where  $c_k$  is the concentration after  $k$  time steps,  $d$  is the delay (the nearest integer of  $\tau/\Delta t$ ) and  $a$  and  $b$  are parameters. These parameters are related to the continuous model (Beven and Young, 1989) by  $T = V_e/Q = -\Delta t/\ln(-a)$  and  $b = 1 + a$ . Here,  $T$  is a time constant characterizing the resident solute time in the soil and  $\Delta t$  is the sampling rate of 0.5 hour. Several such first-order models may be connected to form complex higher order models. The best models have been selected from a range of model orders, including structures allowing for parallel, serial and mixed connections using the simplified refined instrumental variable (SRIV) parameter estimation algorithm (Young, 1984). The

selection was based on the Young information criterion (YIC, Young, 1984) taking into account model error (residual variance) and the number of estimated parameters

$$YIC = \log\left(\frac{\sigma}{\sigma_y}\right) + \log\left(\frac{1}{nm} \sum \frac{\sigma^2 p_{ii}}{\hat{a}_i^2}\right)$$

Here  $\sigma^2$  is the sample variance of the model residuals and  $\sigma_y^2$  is the sample variance of the measured system output  $c_k$  about its mean value. Furthermore,  $nm$  is the total number of parameters estimated,  $a_i$  is the estimate of the  $i$ th parameter in the parameter vector  $\mathbf{a}$  and, finally,  $p_{ii}$  is the  $i$ th diagonal element of a matrix  $\mathbf{P}(N)$  that is related to the estimation error covariance matrix and  $N$  is the sample size.  $YIC$  was used in conjunction with  $r^2$ , here, a goodness-of-fit measure ( $r^2 = 1 - \sigma^2/\sigma_y^2$ ).

#### Soil description and experimental set up

We report here on experiments on two cores from different field sites. Core A was from Lancaster University field station. The soil is a silty loam under permanent grassland and the sample was taken from 15 to 35 cm below the soil surface by first carefully driving a plastic cylinder into the soil. The cylinder was then exposed by manually excavating around it. Finally, the cylinder, containing the soil, was sheared at the base and removed to the laboratory. The other core (core B) was taken from the field station of the Department of Soil and Water Sciences at the Agricultural University of Norway. This is a loam soil also under permanent grassland. The sample was extracted from 20–40 cm below the surface and was sampled using the same procedure as for core A. Table I shows the characteristics of the two cores. Each core is not treated as representative of each site, they have been selected here to illustrate different hydraulic characteristics.

Table I. Dimensions and particle size distribution of soils A and B. Particle size data from Nick Chapell (core A) and Lars Egil Haugen (Core B) (personal communication)

Site	Length (cm)	Diameter (cm)	Sand (%) (0.06–2 mm)	Silt (%) (0.002–0.06 mm)	Clay (%) (<0.002 mm)
Hazelrigg (core A)	17	10.1	41	41	17
Ås (core B)	23	11.7	8	71	21

As stated earlier, ERT may be used to compute internal breakthrough curves (BTCs) of solute transport in the core. Using a peristaltic pump, a saline solution was uniformly distributed on to the upper surface of a vertical standing core. Both cores were saturated before the experiment to give approximately the same initial conditions, i.e. starting from a drainage position. After obtaining steady-state infiltration with a 0.01 M KCl background solution (1.2 dS m<sup>-1</sup>), a 0.05 M KCl solution (6.5 dS m<sup>-1</sup>) was applied at the same rate as a tracer. During infiltration of the tracer, measurements using ERT were taken at selected times. The electrical conductivity of the effluent was measured with a conductivity probe and monitored using a Campbell Scientific Measurements Inc. CR10 datalogging system.

## RESULTS

### Comparing CT and ERT

Investigation of the sequence of CT images, from the top to the bottom of the cores, reveals an increase in density from the top to the bottom of core A, but only two macropores were connected throughout the whole profile. Core B has more macropores consistently through all cross-sections, but small changes in density in the vertical direction. The most distinct feature, however, in core B is a large stone at about 15 cm depth. Figure 2 shows examples of a cross-section from the two cores used in the tracer study from CT. We can

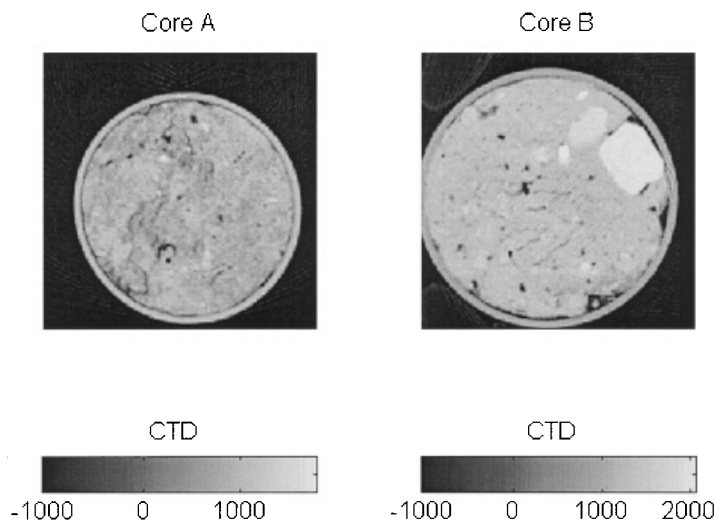


Figure 2. CT images of cores A and B. The images are mapped on a  $256 \times 256$  grid where the pixel dimension is 0.52 mm. The CTD values are shown on the grey level scale

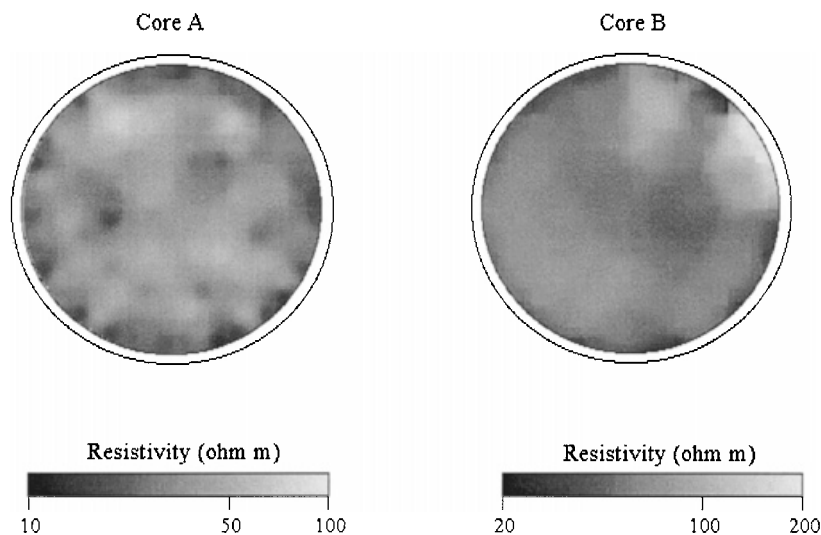


Figure 3. ERT images of core A and B in plane 4 from the base. Corresponds to the depth of the CT images. The resistivity values are shown on the grey level scale

clearly see the stone near the circumference in core B. This stone is also detected in the ERT images as a very high resistivity area (Figure 3). Note the difference in resistivity scales for the two images. In the ERT images the resolution is coarser and the area is smeared out, hiding the exact boundaries of the stone. The stone was present both in plane 4 and plane 5 (plane 1 is the base and plane 10 is the top of the core) which lie between 13.8 and 16.1 cm from the top. The individual macropores are too small to be detected by ERT (Figure 3). The resulting pixel size in the CT images with our soil columns was  $0.52 \text{ mm} \times 0.52 \text{ mm}$  and each pixel was a mean of a 4-mm slice resulting in a voxel size of  $1.1 \text{ mm}^3$ , while in the ERT images the voxels in core A are about  $(0.77 \times 1.7) \text{ cm}^3$  and  $(1.0 \times 2.3) \text{ cm}^3$  in core B.

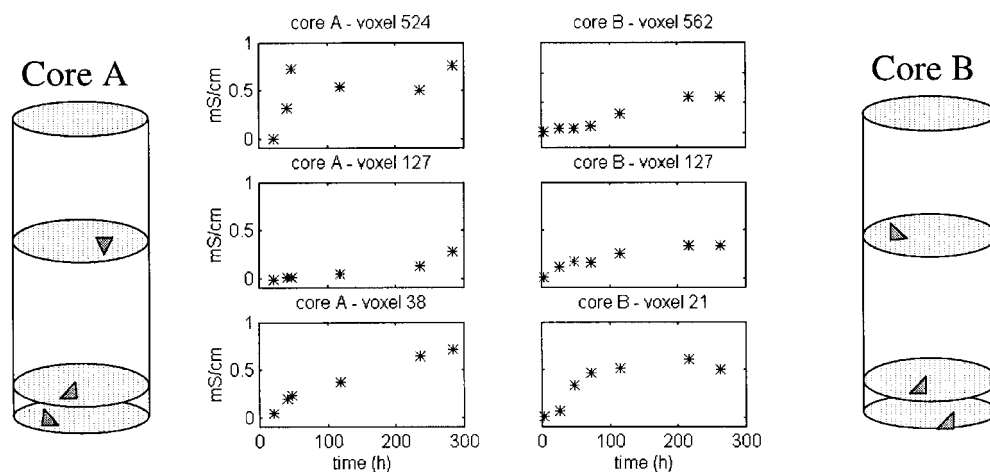


Figure 4. Examples of voxel BTCs in cores A and B. The positions of the voxels are shown approximately at the sides

#### Breakthrough curves

A steady-state infiltration of a 0.01 M KCl solution was assumed when the measured exit flux and the conductivity of the effluent were constant. Steady-state infiltration was measured at the exit as  $7.6 \pm 0.1 \text{ cm}^3 \text{ h}^{-1}$  for core A and  $13.2 \pm 0.4 \text{ cm}^3 \text{ h}^{-1}$  for core B, which resulted in a flux of  $0.095 \pm 0.001 \text{ cm h}^{-1}$  and  $0.120 \pm 0.004 \text{ cm h}^{-1}$ , respectively. Both cores were very moist, but no solute was ponding on the surface.

Examples of some voxel BTCs are shown in Figure 4. The voxels are numbered from 1 to 1040 starting at the bottom plane. For core A voxel 38 is in the first plane, voxel 127 in the second and voxel 524 in the fourth plane. Voxels from the same planes are shown for core B. We see that some voxels (for instance voxel 524 in core A) follow an expected rise in conductivity, while some respond very slowly (core A, voxel 127). Generally, the voxels near the inlet responded faster than the voxels near the exit, with some exceptions. In core B many voxels near the exit responded much faster than voxels near the inlet. For instance, compare the responses of voxels 562 and 21 in Figure 4. The electrical conductivity change thus gives us a three-dimensional distribution of the tracer movement at different times.

The aggregated profile conductivity plots showing the vertical distribution of the change in conductivity are displayed in Figure 5. Here we see the difference in response of the two cores. Core A has a continuously decreasing concentration from the top to the bottom. In core B, however, the bottom plane responds very fast, suggesting preferential flow. The concentration in each plane is increasing with time as expected. The variation of the initial conductivities in each plane in core A was small compared with the change owing to the tracer. In core B there was initially a large variation in the conductivities in planes 4 and 5, where the stone was present, while the other planes had a similar variation to core A. It is interesting to note that the conductivity change in the bottom plane of core A never reaches the same level as the top plane. The reason for this is that part of the exit area is not responding to the tracer, as demonstrated in Figure 6 where the frequency distributions of electrical conductivity 236 and 216 hours after tracer injection for core A and B respectively, are shown. The ordinate gives the number of voxels with a certain change in electrical conductivity. Core A has a rather symmetrical distribution near the top of the core. Further down the distribution is skewed so that some voxels hardly respond while a few have large responses. In core B the distribution is skewed in all planes, indicating two transport modes.

Figure 7 shows the BTCs measured with the conductivity probe, expressed as a reduced concentration calculated as the change in measured conductivity divided by the total change. Using the transfer function approach suggested by Beven and Young (1988) the best model for core A ( $YIC = -15.93$ ) was a first-order

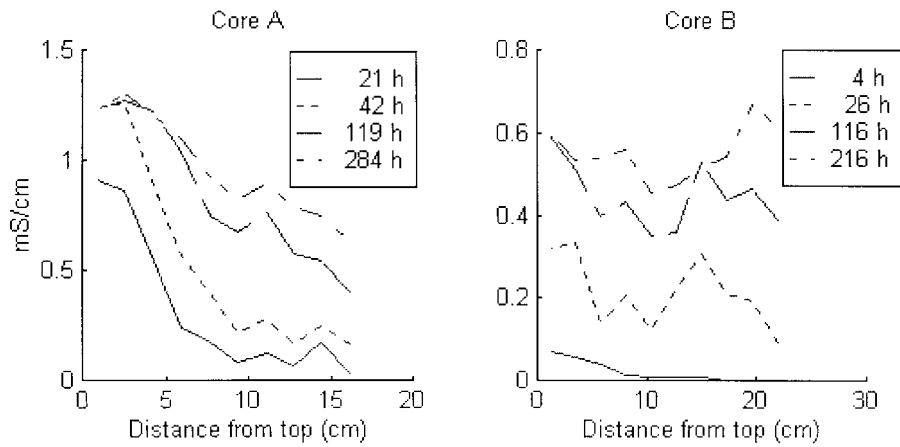


Figure 5. Aggregated profile conductivity plot showing the vertical distribution of the changes in bulk electrical conductivity at selected times

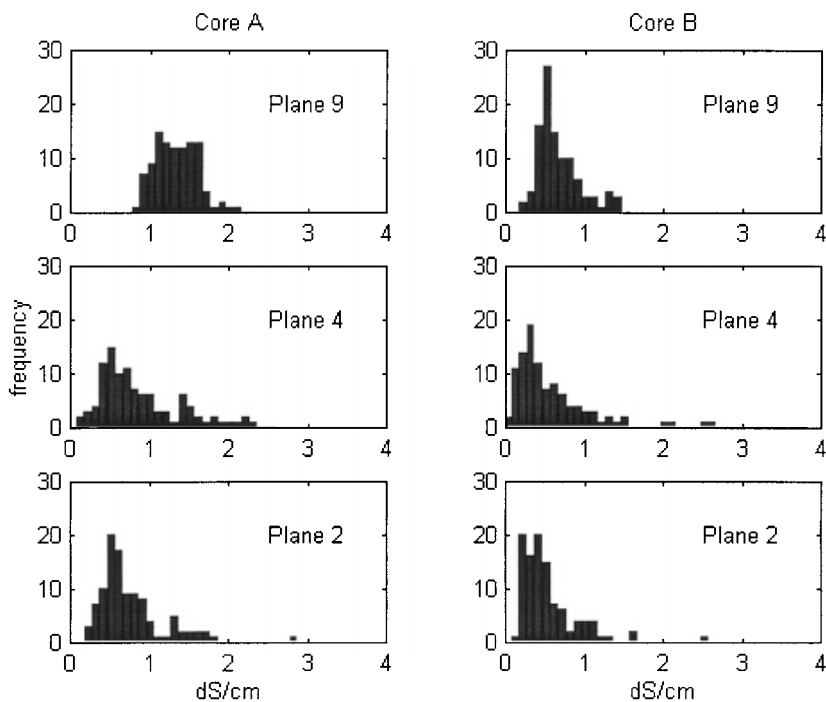


Figure 6. Frequency distribution of bulk electrical conductivity changes in some planes in core A at 236 and core B at 216 hours after tracer injection. Plane 9 is the second plane from the source (starting 1.7 cm and 2.3 cm from the source in cores A and B, respectively) and plane 2 is near the bottom (starting 13.6 cm and 18.4 cm from the source in core A and B, respectively)

model ([1,0,26]) with  $\mathbf{a} = [1, -0.9864]$ ,  $\mathbf{b} = 0.0138$  and  $d = 26$ . This means that there is no evidence in the measured data of parallel flow mechanisms. The best model of core B ( $YIC = -15.18$ ) was a second order model ([2,1,17]) with real roots of the denominator  $\mathbf{a} = [1, -1.9269, 0.9275]$ ,  $\mathbf{b} = [0.0231, -0.0226]$  and  $d = 17$ ). This model may then be decomposed into two first-order models in parallel and hence suggests that there are two parallel flow mechanisms (according to our measured effluent data).

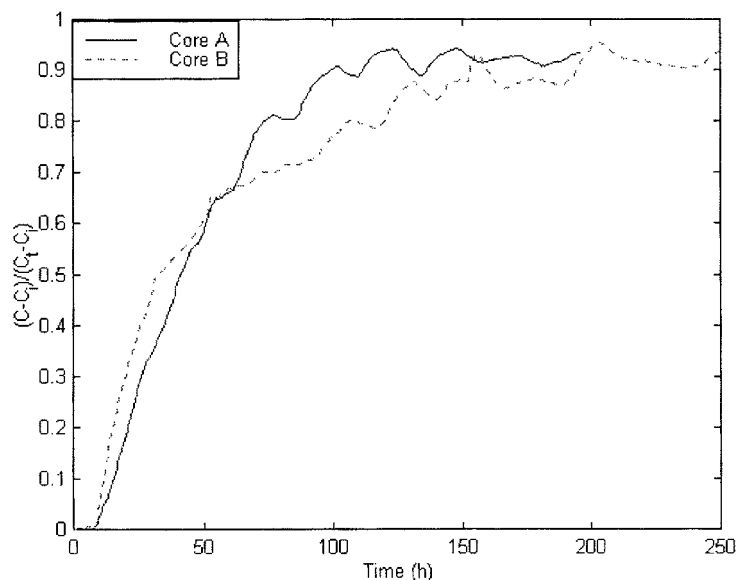


Figure 7. Effluent breakthrough of solute measured with conductivity probe and logged every 30 minutes presented as reduced concentrations.  $C$  is measured conductivity,  $C_i$  initial conductivity and  $C_t$  tracer conductivity

The resulting time constant for core A is  $T = 36.5$  h, which gives an effective volume of transport of  $V_e = QT = 7.6 \text{ cm}^3 \text{ h}^{-1} \times 36.5 \text{ h} = 277 \text{ cm}^3$ . The total volume is  $1362 \text{ cm}^3$ , which gives an effective fractional transport volume of 0.20. Our sampling rate was every 30 minutes, so the time delay  $d = 26$  means a transport delay of 13 hours. For core B we have two time constants  $T_1 = 61$  hours and  $T_2 = 7.5$  hours. The ratio of the two steady-state gains in the model is 2.8503, which enables us to separate the flow in the two domains as  $Q_1 = 9.77 \text{ cm}^3 \text{ h}^{-1}$  and  $Q_2 = 3.43 \text{ cm}^3 \text{ h}^{-1}$ . Together with the time constants and the total soil volume of  $2473 \text{ cm}^3$  we can estimate the fractional transport volumes as 0.21 and 0.011 for modes 1 and 2, respectively. The slow mode is transported through 21% of the soil volume while the fast mode is only transported through 1.1%. The time delay  $d = 17$  suggests a transport delay of 8.5 hours.

## DISCUSSION

We see from the CT images and the initial ERT images that CT provides better resolution. The stone in core B is clearly seen in the CT image. The ERT image has an area with a very high resistivity in that region, but it is smeared out and it is difficult to see the actual shape of the stone. The tracer, however, causes a significant change in the bulk electrical conductivity and the response in the individual voxels and the mean response of each plane is distinct. It appears that the tracer bypasses some areas in both cores. This is consistent through all of core B, but is apparent only for the bottom half of core A. The aggregated profile conductivity plots in Figure 5 measured with ERT are consistent with the effluent BTCs in Figure 7. The fast response of the bottom planes of core B and the skewed distribution of electrical conductivity changes suggest some kind of preferential flow mechanism, which was also discovered using the transfer function approach on the effluent conductivity data. The parallel transport modes detected in core B are perhaps a result of the greater number of macropores. However, this could not be verified with the ERT measurements because of the coarse resolution.

The sampling time for the ERT measurements was 4.5 hours for the whole core. With the measured flux of about  $0.1 \text{ cm h}^{-1}$  and effective transport volumes of approximately 0.2, the effective velocity is about

0.5 cm h<sup>-1</sup> and thus in 4.5 hours the solute has travelled about 2.3 cm. This will give a shift in the aggregated conductivity profiles, but considering the time to reach the final concentration level of 150–200 hours (Figure 7) we expect this error to be small. The peak in the aggregated conductivity profile plots in plane 4 in core B (Figure 5) 26 and 116 hours after tracer injection was partly a result of large changes in two voxels near the stone. This could be a consequence of increased water content (as well as fluid conductivity), for instance as a result of colloid transport that temporarily clogged some pores. The larger variation in the measured water flux at the exit of core B than at the exit of core A supports this. However, the variations were small in both cases and approximate steady-state flow is assumed.

The transfer function model only assumes a linear system. When estimating transport parameters further assumptions, such as the conservation of mass, are required. If an additional assumption of complete transverse mixing of solute is added, the classical convection dispersion equation can be applied. The program CXTFIT (Toride *et al.*, 1995) analyses one-dimensional steady-state flow of solutes with several types of convection dispersion equation (CDE) and permits estimations of transport parameters. Our experiment was designed to obtain one-dimensional steady-state flow and we thus fitted the effluent conductivity data to equilibrium and physical non-equilibrium CDEs. The physical non-equilibrium CDE is also called the mobile-immobile CDE. The effluent data of both core A and B fit the equilibrium CDE well ( $r_A^2 = 0.9949$  and  $r_B^2 = 0.9896$ , respectively). The non-equilibrium CDE gives approximately the same fit as the equilibrium CDE ( $r_A^2 = 0.9887$  and  $r_B^2 = 0.9911$ ), but the mobile water fraction is nearly one ( $\beta_A = 0.999$  and  $\beta_B = 0.967$ ) in both cases. This implies that the equilibrium CDE is the best model for core A. The large fraction of mobile water and the small increase in the fit suggests that the equilibrium CDE is just as good as the non-equilibrium CDE for core B also.

Using the fitted parameters in the best CDEs to predict the concentrations in the bottom plane of core A and B and compare these with the ERT measurements at different times gave no satisfactory results. The CDE equation overestimates the concentration compared with the ERT measurements. In Figure 6 we see that parts of the bottom planes have almost no change in solute concentration. The average concentrations of these planes are clearly smaller than in the solute conductive zones. The CDE is perhaps not the correct process model to employ here as it assumes complete transverse mixing, i.e. a mixing time in the lateral direction that is faster than that in the vertical. The fundamental opposite process model is that solute is transported in regions with no lateral exchange of solute between the regions. This is frequently called a stochastic convective model. It is assumed that solute flow starts as a stochastic convective flow and gradually transforms into a convective dispersive flow after some distance (Dürner and Flüßler, 1996; Jury and Roth, 1990).

Cores of the size of those described here do not reflect the spatial variability in a field and care should be taken in extrapolating these results to the field scale.

## CONCLUSIONS

CT is clearly superior in resolution performance when compared with ERT. The flexibility of ERT, however, allows us to look at bulk changes for long time periods and on larger scales. The results presented show how relatively new tomographic imaging techniques can be used to add information about the transport characteristics of soils in a non-invasive manner. We have presented breakthrough curves (BTCs) in three dimensions. Our experiment was aimed at obtaining a one dimensional flow which was reflected in conductivity profiles using aggregated voxel resistivities for each plane. These profiles were able to explain the observed effluent BTCs qualitatively. Further work must explore how these internal geoelectric patterns can be used to obtain quantitative information about transport processes.

Even if the effluent BTC shows a classical behaviour and fits some type of the CDE, the ERT images show that the internal solute distribution is very complex and the fitted parameters do not necessarily have a physical meaning.

## ACKNOWLEDGEMENTS

This work has been supported by funding from the European Groundwater Research Network (EUGREP, European Commission, grant number ERB CHRX CT92 0074). The first author was also supported by a travel grant (no. 116146/100) from the Norwegian Research Council. Thanks to Nick Chapell and Lars Egil Haugen for providing soil data.

## REFERENCES

- Amin, M. H. G., Chorley, R. J., Richards, K. S., Hall, L. D., Carpenter, T. A., Cislerova, M., and Vogel, T. 1997. 'Study of infiltration into a heterogeneous soil using magnetic resonance imaging', *Hydrol. Process.*, **11**, 471–483.
- Anderson, S. H. and Hopman, J. (eds) 1994. *Tomography of Soil–Water–Root Processes*, Soil Science Society of America Special Publication Number 36. Soil Science Society of America, Madison, Wisconsin.
- Barber, D. C. and Brown, B. H. 1984. 'Applied potential tomography', *J. Phys. E*, **17**, 723–733.
- Beven, K. and Young, P. C. 1988. 'An aggregated mixing zone model of solute transport through porous media', *J. Cont. Hydrol.*, **3**, 129–143.
- Binley, A., Poulter, S. H., and Shaw, B. 1996a. 'Examination of solute transport in an undisturbed column using electrical resistance tomography', *Wat. Resour. Res.*, **32**, 763–769.
- Binley, A., Pinheiro, P., and Dickin, F. 1996b. 'Finite element based three-dimensional forward and inverse solvers for electrical impedance tomography', in *Proc. Colloquium on Advances in Electrical Tomography*, Computing and Control Division, IEE, Digest No. 96/143, pp. 6/1–6/3.
- Daily, W., Ramirez, A., LaBrecque, D., and Nitao, J. 1992. 'Electrical resistivity tomography of vadose water movement', *Wat. Resour. Res.*, **28**, 1429–1442.
- Dürner, W. and Flühler, H. 1996. 'Multidomain model for pore-size dependent transport of solutes in soils', *Geoderma*, **70**, 281–297.
- European Environment Agency and United Nations Environment Program, 1997. 'Water stress in Europe — can the challenge be met?', *New Year Message 1997*. EEA and UNEP, Copenhagen. 15 pp.
- Jury, W. A. and Roth, K. 1990. *Transfer Functions and Solute Movement through Soil*. Birkhauser Verlag, Basel. 226 pp.
- Parker, J. C. and van Genuchten, M. Th. 1984. 'Flux averaged and volume averaged concentrations in continuum approaches to solute transport', *Wat. Resour. Res.*, **20**, 866–872.
- Slater, L., Brown, D., and Binley, A. 1996. 'Determination of hydraulically conductive pathways in fractured limestone using cross-borehole electrical resistivity tomography', *Eur. J. Environ. Engng Geophys.*, **1**, 35–52.
- Toride, N., Leij, F. J., and van Genuchten, M. Th. 1995. 'The CXTFIT code for estimating transport parameters from laboratory or field tracer experiments, version 2.0', *Research Report 137*. US Salinity Laboratory, Agricultural Research Service, US Department of Agriculture, Riverside, California.
- Young, P. C. 1984. *Recursive Estimation and Time Series Analysis: An Introduction*. Springer Verlag, Berlin. 269 pp.